

# MDMP: Multi-modal Diffusion for supervised Motion Predictions with uncertainty

Leo Bringer, Joey Wilson, Kira Barton, Maani Ghaffari  
University of Michigan

lbringer, wilsoniv, bartonkl, maanigj@umich.edu

## Abstract

*This paper introduces a Multi-modal Diffusion model for Motion Prediction (MDMP) that integrates and synchronizes skeletal data and textual descriptions of actions to generate refined long-term motion predictions with quantifiable uncertainty. Existing methods for motion forecasting or motion generation rely solely on either prior motions or text prompts, facing limitations with precision or control, particularly over extended durations. The multi-modal nature of our approach enhances the contextual understanding of human motion, while our graph-based transformer framework effectively capture both spatial and temporal motion dynamics. As a result, our model consistently outperforms existing generative techniques in accurately predicting long-term motions. Additionally, by leveraging diffusion models' ability to capture different modes of prediction, we estimate uncertainty, significantly improving spatial awareness in human-robot interactions by incorporating zones of presence with varying confidence levels for each body joint.*

## 1. Introduction

Through collaboration and assistance, robots could significantly augment human capabilities across diverse sectors, including smart manufacturing, healthcare, agriculture, and construction. Indeed, they can complement the critical and adaptive decision-making skills of human workers with higher precision and consistency in repetitive tasks. However, one challenge prohibiting human-robot collaboration is the safety of workers in the presence of robots. To act safely and effectively together, continuous knowledge of future human motion and location in the common workspace with a measure of uncertainty is pivotal. This real-time awareness allows robots to adjust their trajectories to avoid collision and perform precise collaborative tasks [5, 25, 58].

Humans can predict future events based on their self-constructed models of physical and socio-cultural systems.

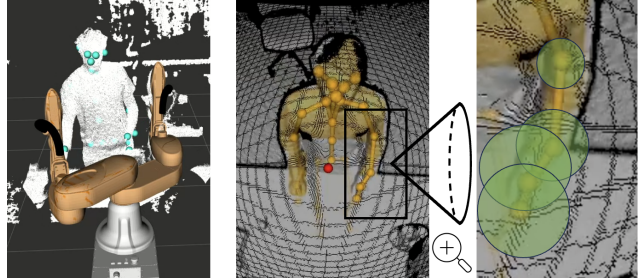


Figure 1. **Application in Human-Robot Collaboration:** Based on the action: "Picking up an object; giving object to the robot" our MDMP predicts the future movements of the human worker with an uncertainty zone of presence around each body joint.

This skill, developed from childhood through observation and active participation in society, enables them to anticipate others' movements. Researchers are now trying to transfer this capability often referred as "Theory of mind" [10] to machines by training them to learn similar motion estimation tasks. Current methodologies fall into two primary categories: Human Motion Forecasting (see Section 2.2) and Human Motion Generation (see Section 2.3). While the former uses only a short input sequence of skeletal motion to predict its future trajectory, the latter relies exclusively on textual prompts to generate motion sequences. Despite advancements in text-to-motion models, challenges remain in controlling generation due to the expansive action space a simple prompt can describe, which may not always align with human expectations or behavior.

Conversely, motion prediction using past sequences is a long-standing challenge that has achieved high accuracy over short-term predictions but struggles with long-term predictions. This is understandable, as even for humans, predicting someone's immediate future movement based on past motions is feasible, but beyond one or two seconds, the variety of possibilities makes it nearly impossible without context. However, knowledge of the intended action provides a rough idea of future positions, as the contextual information of the action guides intuitions.

In Human Robot Collaboration (HRC), there is a crucial

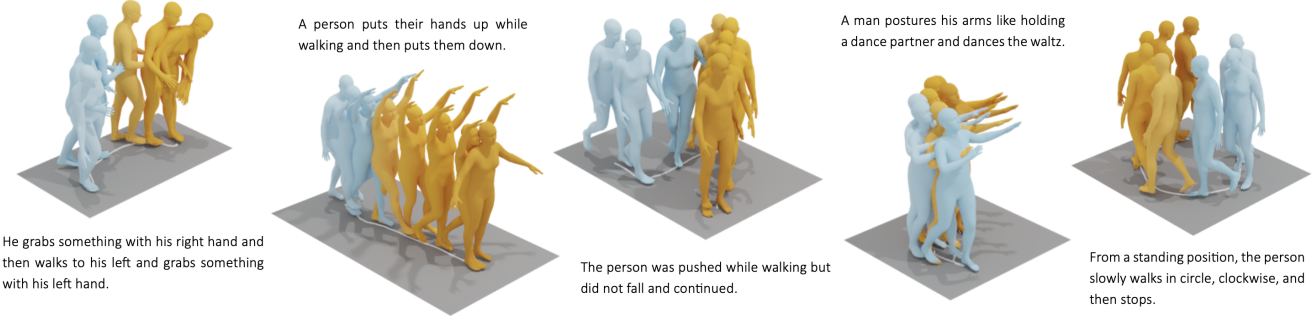


Figure 2. **SMPL Meshes of MDMP Predicted motions of different scenarios.** The text descriptions vertically associated to the motions as well as the blue frames are the inputs of the model. The orange frames are the predictions, darker colors indicate later frames.

need for longer-term predictions to coordinate precise interactive tasks, avoid collisions, and maintain efficient trajectory planning. As a result, our method uniquely combines and synchronizes textual and skeletal data to generate precise, longer-term predictions. Indeed, this integration allows for a richer, more contextually aware generation of motion predictions. To the best of our knowledge, this model is the first to be trained on a combination of both types of inputs to leverage context in motion.

In this work, inspired by MDM [50] (Motion Diffusion Model) and LTD [36] (Learning Trajectory Dependencies), we propose a transformer-based diffusion model with a Graph Convolutional Encoder optimized for the spatio-temporal dynamics of motion data. A key design element is the use of learnable graph connectivity, as introduced by Mao et al. [36], to more effectively capture joint dependencies. Our model is trained in a classifier-free manner [18], allowing for a balance between variability and accuracy, with an emphasis on precision to ensure safety in HRC. Additionally, our Multi-modal Diffusion Model for Motion Predictions (MDMP) harnesses the stochastic nature of diffusion models to predict presence zones with varying confidence levels. This uncertainty measure is particularly crucial for long-term motion predictions, where uncertainty grows over time. By offering a spatial understanding of human presence, our model significantly enhances collision avoidance, improving safety and real-time interaction in dynamic collaboration scenarios.

We summarize the contributions as follows: 1) A novel multi-modal diffusion model integrating textual and skeletal data to generate long-term motion predictions. 2) A graph-based transformer framework that effectively captures spatial and temporal dynamics of motion. 3) A method for estimating uncertainty in predictions, improving spatial awareness and safety in HRC scenarios. 4) A thorough validation of the predicted uncertainty through a comparative study and finally our implementation is open-sourced.

## 2. Related Work

In this section, we review key works that inform our approach. We cover Diffusion Generative Models, Human Motion Forecasting, and Human Motion Generation, highlighting the advancements and limitations in each area as they relate to our method.

### 2.1. Diffusion Generative Models

Diffusion models [17,46,47] are neural generative models based on a stochastic diffusion process as modeled in Thermodynamics. The training process involves two phases: forward and backward. The forward process takes observed samples  $x$  and progressively adds Gaussian noise until the original information is completely obscured. In contrast, the backward or reverse process employs a neural model that learns to denoise a sample from pure noise back to the original data distribution  $p(x)$ , hence the term Denoising Diffusion Probabilistic Models [17]. DDPMs have gained prominence in generative modeling, initially demonstrating excellent performance in image generation, and later in conditioned generation [9] and latent text representation [40] using CLIP [44]. Recently, diffusion models have also been applied to various generation tasks, such as text-to-speech [43], text-to-sound [56], and text-to-video [19].

While diffusion models excel in performance, a significant trade-off is the lengthy inference time required for the reverse process, which is impractical for real-time applications. However, many work such as DDIM [48] and Consistency Models [49] tackles that issue and trade off computation for sample quality. Nichol et al. [39] found that instead of fixing variances of distributions modeling the progressively denoised data as a hyperparameter [17], learning it would improve log-likelihood, forcing generative models to capture all data distribution modes, and enable faster sampling with minimal quality loss. Considering the paramount importance of efficiency in HRC, we follow Nichol et al.’s

approach by learning variances and leverage the different modes as a factor for uncertainty. Our method demonstrates better performance with just 50 time steps instead of 1000, achieving over 20 times faster inference.

## 2.2. Human Motion Forecasting

Human Motion Forecasting aims to predict future full-body motion trajectories in 3D space based on past observations from motion capture data or real-time Human Pose Estimation methods. This task is formulated as a sequence-to-sequence problem, using past motion segments to predict future motion. Deep learning methods have shown notable results due to their ability to learn motion patterns and understand spatio-temporal relationships. Early methods employed RNNs [11, 20, 26, 32, 37], then CNNs [31, 57] and GANs [7, 12, 16, 22, 27, 53, 60] but either accumulated errors led to unrealistic predictions or faced limitations due to pre-fixed kinematic dependencies between body joints. GCNs have proven effective for the task [8, 29, 30, 33, 36, 59], considering that the human skeleton can be effectively modeled as a graph. Transformer-based models, leveraging self-attention [51] for long-range dependencies, have also been adopted [2, 4, 38, 54]. Considering the efficiency and accuracy of the previously mentioned methods, our denoising model leverages GCNs to encode joint features due to their effectiveness in capturing spatial patterns, and a Transformer backbone in the latent space to address the temporal nature of motion data. However, since none of these methods can learn contextual information from the data they are fed, they tend to diverge for durations beyond one second.

## 2.3. Human Motion Generation

Instead of predicting future motion based on past sequences, some generative methods are conditioned natural language [1, 41] to overcome this short-term issue. This approach faces other challenges such as the vast variability of possible motions corresponding to the same label. However, Text2Motion has garnered significant interest and varied successful approaches. TEMOS [41] and T2M [14] employ a VAE to map text prompts to a latent space distribution of language and motion. MotionGPT [21] furthers this by proposing a unified motion-language framework. Recently, MDM [50] leveraged recent advancements in DDPMs, proving that diffusion models are a better candidate for human motion generation, as they can retain the formation of the original motion sequence and thus allows them to easily apply more constraints during the denoising process. LDM [6] took it forward by performing Diffusion in the latent space and MoMask [13] & MMM [42] leverages Masked Transformers.

By fixing some parts of a motion sequence and filling in the gaps, some of these Text2Motion baselines such as MDM [50] and MotionGPT [21] propose a form of "mo-

tion editing" by forcing their models to generate motions with preserved original data. Unlike these methods, which only edit motions during sampling, our approach trains the model with both textual prompts and motion sequence conditioning to learn contextuality and guide generation towards precise predictions. While these models are compared on diversity and multi-modality metrics, our goal is to minimize the distance between predictions and ground-truth for accurate predictions in HRC.

## 3. Methodology

We now explain the architecture of our proposed MDMP in detail. For an overview, please refer to Figure 3. Our method uses the building blocks of MDM [50], but with three main differences: (1) a denoising model that includes variance learning to increase log-likelihood and perform uncertainty estimates, (2) a GCN encoder with learnable graph connectivity, and (3) a learning framework that incorporates contextuality by synchronizing skeletal inputs with initial textual inputs.

### 3.1. Problem Formulation

A motion sample can be represented by a temporal skeleton sequence  $X = \{p^i\}_{i=1}^N$  where a frame  $p_i$  denotes a pose that can be modeled using different joint feature representations depending on the dataset (see Section 4.1). The simplest form that any representation can easily revert to without any loss of information is the joints' position in 3D space where  $p_i = \{x(1)_i, \dots, x(J)_i\}$  with joints  $x(j) \in \mathbb{R}^M$  where  $M = 3$  and  $J$  being the total number of joints. Some parameterizations use rotation matrices ( $M = 9$ ), angle-axis ( $M = 4$ ), or quaternion ( $M = 4$ ) to represent each joint, while others include information such as angular and/or linear velocity.

Our goal is to generate a motion sample conditioned on both a prefix of that sequence  $Y = \{p^i\}_{i=1}^n$  with  $n < N$  and a textual prompt that will be encoded into a textual embedding  $c$  by CLIP [44].

### 3.2. The Variational Diffusion Process

A Diffusion model can be described as a Markovian Hierarchical Variational Auto-Encoder [34] with a constant latent dimension. During training, we draw  $X_0$  from the data distribution, and at each time step  $t$ , the fixed encoder adds linear Gaussian noise centered around the output of the previous latent sample  $X_{t-1}$  until its distribution becomes a standard Gaussian at the final time step  $T$ . Hence, the Gaussian encoder is parameterized with mean  $\mu_t(X_t) = \sqrt{\alpha_t}X_{t-1}$  and variance  $\Sigma_t(X_t) = (1 - \alpha_t)I$ :

$$q(X_t|X_{t-1}) = \mathcal{N}(X_t; \sqrt{\alpha_t}X_{t-1}, (1 - \alpha_t)I) \quad (1)$$

$$q(X_{1:T}|X_0) = \prod_{t=1}^T q(X_t|X_{t-1}) \quad (2)$$

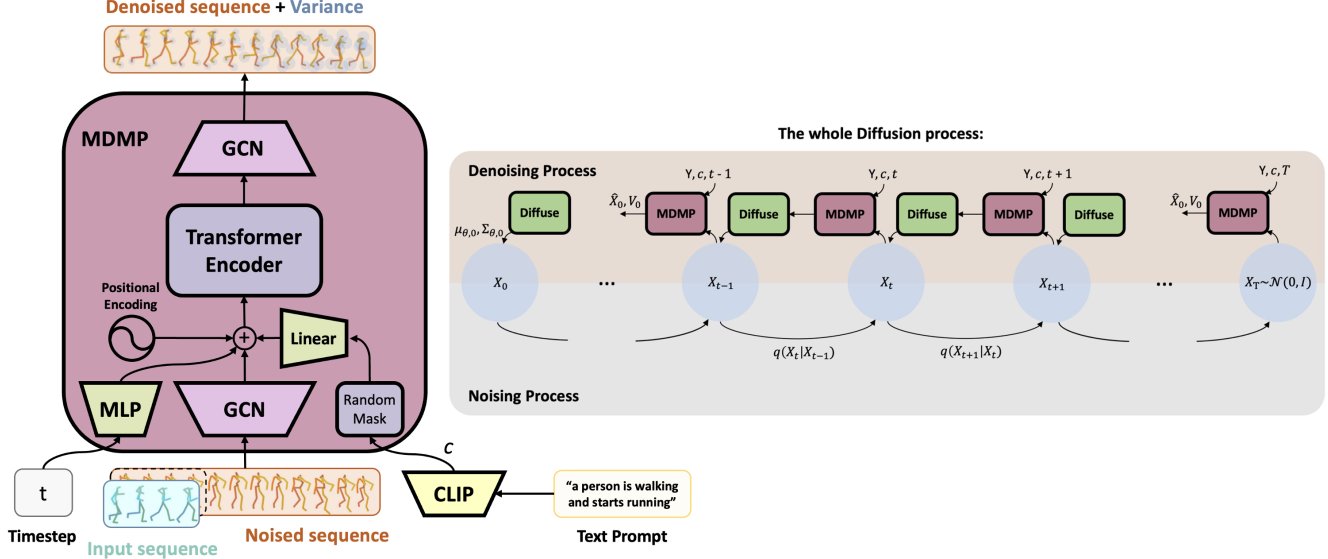


Figure 3. **(Left) Architecture of MDMP.** The denoising model takes as input a motion sample  $X_t = \{p_t^i\}_{i=1}^N$  from the previous latent distribution, the diffusion time step  $t$  and the conditioning parameters:  $Y = \{p^i\}_{i=1}^n$  with  $n < N$  the motion input sequence and  $c$  the textual embedding encoded by CLIP [44]. At each time step, MDMP outputs a prediction of the final motion  $\hat{X}_0$  along with  $V_0$ , the variance of each predicted joint feature. **(Right) Overview of the Diffusion Process.** On top is the denoising Process, where the Sampling starts from  $t = T$  and recursively calls MDMP and uses the output along with  $X_t$  to diffuse back to  $X_{t-1}$  by calculating  $\mu_{\theta, t}$  and  $\Sigma_{\theta, t}$ .

Inspired by Nichol et al. [39], we use a cosine scheduler for  $\beta_t$  and  $\alpha_t = 1 - \beta_t$  such that  $\beta_t, \alpha_t \in [0, 1]$ .  $\alpha_t$  is slowly decreasing, so that for  $T = 1000$ ,  $\alpha_t$  is small enough to say that  $X_T \sim \mathcal{N}(0, I)$ .

Then, during both training and inference, we use MDMP (see Fig. 2a) as the decoder—conditioned at each step by the previously mentioned inputs  $Y$  and  $c$ —to progressively denoise  $X_t$  from a standard Gaussian. Instead of predicting the noise  $\epsilon_0$  as formulated in DDPM [17], we follow [45] and [50] and predict the signal itself along with its variance:  $\hat{X}_0, V_0 = \text{MDMP}(X_t, t, Y, c)$

Then we use this prediction  $\hat{X}_0$  along with the current  $X_t$  to diffuse back to the posterior mean:

$$\mu_{\theta, t-1} = \frac{\sqrt{\alpha_t}(1 - \bar{\alpha}_{t-1})X_t + \sqrt{\bar{\alpha}_{t-1}}(1 - \alpha_t)\hat{X}_0}{1 - \bar{\alpha}_t} \quad (3)$$

$$\text{with } \bar{\alpha}_t = \prod_{s=1}^t \alpha_s. \quad (4)$$

We use the simple objective from [17] to train our model:

$$L_{\text{simple}} = \mathbb{E}_{X_0 \sim q(X_0 | c, Y), t \sim [1, T]} \left[ \|X_0 - \hat{X}_0\|^2 \right] \quad (5)$$

One subtlety is that  $L_{\text{simple}}$  provides no learning signal for variances, as Ho et al. [17] chose to fix the variance rather than learn it. However, in our specific application, we leverage learned variances to generate presence zones with varying confidence levels to help ensure safety in HRC scenarios.

### 3.3. Learning the Variances of the Denoising process

To learn the reverse process variances, our model outputs a vector  $V_0$  of the same shape as  $\hat{X}_0$ , and—following Nichol et al. [39]—we parameterize the variance as an interpolation between  $\beta_t$  and  $\tilde{\beta}_t$  in the log domain by turning this output  $V_0$  into  $\Sigma_{\theta, t}$  as follows:

$$\Sigma_{\theta, t} = \exp(V_0 \log \beta_t + (1 - V_0) \log \tilde{\beta}_t) \quad (6)$$

$$\text{with } \tilde{\beta}_t := \frac{1 - \bar{\alpha}_{t-1}}{1 - \bar{\alpha}_t} \beta_t. \quad (7)$$

Then, we leverage the reparameterization trick  $x_t = \bar{\alpha}_t x_0 + \sqrt{1 - \bar{\alpha}_t} \epsilon$  with  $\epsilon \sim \mathcal{N}(0, I)$  to sample from an arbitrary step of the forward noising process and estimate the variational lower bound (VLB). As mentioned earlier, the diffusion model can be thought of as a VAE [23] where  $q$  represents the encoder and  $p_{\theta}(x_{t-1} | x_t) = \mathcal{N}(x_{t-1}; \mu_{\theta, t}, \Sigma_{\theta, t})$  is the decoder, so we can write:

$$L_{\text{VLB}} := L_0 + L_1 + \dots + L_{T-1} + L_T \quad (8)$$

$$L_0 := -\log p_{\theta}(x_0 | x_1) \quad (9)$$

$$L_{t-1} := D_{\text{KL}}(q(x_{t-1} | x_t, x_0) \| p_{\theta}(x_{t-1} | x_t)) \quad (10)$$

$$L_T := D_{\text{KL}}(q(x_T | x_0) \| p(x_T)) \quad (11)$$

Finally, with  $q(x_{t-1} | x_t, x_0) = \mathcal{N}(x_{t-1}; \tilde{\mu}(x_t, x_0), \tilde{\beta}_t I)$  we estimate  $L_{t-1}$  and approximate  $L_{\text{VLB}}$  with the expectation  $\mathbb{E}_{t, X_0, \epsilon}[L_{t-1}]$ .

Since  $L_{\text{simple}}$  does not depend on  $\Sigma_{\theta,t}$ , we define a new hybrid objective:  $L_{\text{hybrid}} = L_{\text{simple}} + \lambda L_{\text{VLB}}$

Conversely to Nichol et al. [39], we apply a clamping on  $V_0$  to prevent NaN values during the calculation of  $L_{\text{VLB}}$ .

### 3.4. Encoding the joint features

To encode the spatial structure of the pose features, we leverage GCNs [52]. Instead of relying on a predefined sparse graph, we follow Mao et al. [36] and learn the graph connectivity during training, thus essentially learning the dependencies between the different joint trajectories. To this end, we model the human body through the joint features as a fully-connected graph with  $K$  nodes. The strength of the edges in this graph can then be represented by a weighted adjacency matrix  $A \in \mathbb{R}^{K \times K}$ . The graph convolutional encoder/decoder then takes as input a matrix  $H^{(\text{in})} \in \mathbb{R}^{K \times F}$ , with  $F$  the number of features. In our case, the encoder takes as input the  $K \times N$  matrix of joint features for each frame  $n \in [0, N]$  of the sequence. Given this information and a set of trainable weights  $W \in \mathbb{R}^{F \times \hat{F}}$ , a graph convolutional layer outputs a matrix of the form:  $H^{(\text{out})} = AH^{(\text{in})}W$ . Where  $A$  is the trainable weighted adjacency matrix. All operations are differentiable with respect to both  $A$  and  $W$ , which allows training on both the weights and the joint feature connectivities.

### 3.5. Predicting Uncertainty

To derive an effective uncertainty index for each joint prediction over time, we explore three different approaches which we evaluate and compare in Section 4.4:

- **Mode Divergence:** This approach measures the variability between multiple motion sequences generated from the same input. We compute several predictions in parallel, calculate the standard deviation of these sequences, and use this as the uncertainty index.
- **Denoising Fluctuations:** Here, we measure the fluctuations during the denoising process as an uncertainty indicator. As illustrated in Figure 1 which tracks the evolution of the x-coordinate of key joints (head, hands, feet) from random noise to the final prediction, earlier steps are very noisy and progressively converge with more or less stability. Significant fluctuations in the last 20 timesteps are used as an indicator of uncertainty.
- **Predicted Variance:** The final approach leverages the variance of the predicted distribution of each motion sequence  $\Sigma_{\theta,0}$  learned during training.

Both the second and third methods produce outputs in the same dimensions as the model, including predictions for root height, root angular and linear velocity, as well as

joint positions and velocities in the local reference of the root. To calculate a single uncertainty index for each joint at each timestep, we average all features associated to the same joint.

### 3.6. Model Specifics

As shown in Figure 3, upstream of the encoder, the motion sample  $X_t = \{p_t^i\}_{i=1}^N$  is conditioned by the input motion  $Y = \{p^i\}_{i=1}^n$  through masking. The noise time-step  $t$  and the textual embedding  $c$  are projected to the same dimensional latent space by separate feed-forward networks. These features, summed with a sinusoidal positional embedding, are fed to the transformer encoder-only backbone [51]. The backbone output is projected back to the original motion dimensions and serves as the prediction. When learning variances, joint features are encoded in a latent space with twice the dimensions to decode  $\hat{x}_0$  and their associated variance  $V_0$  separately. Our model is trained both conditionally and unconditionally on text, by randomly masking 10% of the text embeddings. This allows to balance diversity and text-fidelity during sampling (see Figure 3 (Right)).

## 4. Experiments and Results

In this section, we present the experimental setup and evaluation of our proposed model. We describe the dataset used for training and testing, outline the metrics for accuracy and uncertainty, and provide details on our model’s implementation. Finally, we present a comprehensive quantitative and qualitative evaluation, including comparisons with Text2Motion baselines that propose Motion-Editing, analysis of uncertainty parameters, and an ablation study to assess the effects of motion-text fusion and architectural design choices.

### 4.1. Dataset

To train and evaluate our model, we use the HumanML3D [14] dataset, which is the largest and most diverse collection of scripted human motions. It combines motion sequences from the HumanAct12 [15] and AMASS [35] datasets, processed to standardize the motions to 20 FPS with a maximum length of 10 seconds per sequence. HumanML3D comprises 14,616 motions with 44,970 descriptions, covering 5,371 distinct words, totaling 28.59 hours of motion data with an average length of 7.1 seconds and three textual descriptions per sequence. The dataset is split for training and evaluation. For evaluation, we filter the set to include only motions longer than 3 seconds, allowing us to condition the models on 2.5 seconds of motion and predict at least 0.5 seconds into the future. After filtering, the evaluation set contains 4,328 out of the initial 4,646 motion sequences.

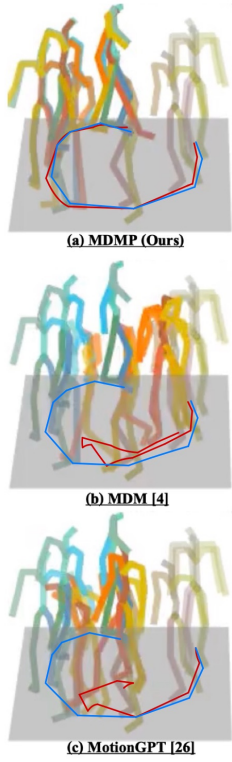
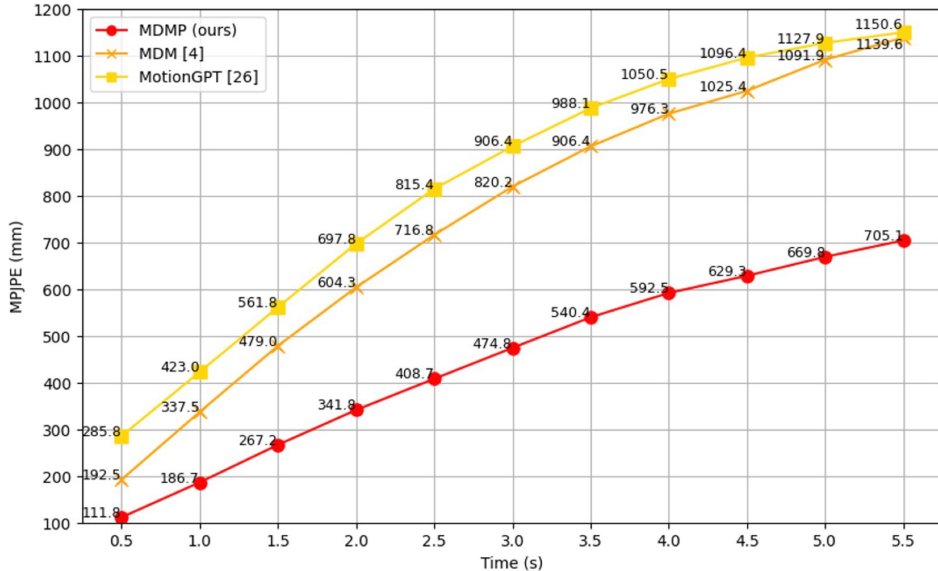


Figure 4. **(Left)** Temporal evolution of error in predictions. Quantitative Results on HumanML3D over MPJPE [mm]. **(Right)** 3D Plots of Motion Predictions (orange) vs Ground truth (blue). Motion Sequence example associated to textual prompt: “from a standing position, the person slowly walks in circle, clockwise, then stops”. Paler shades represents earlier frames.

## 4.2. Metrics for Accuracy and Uncertainty

To evaluate and compare the accuracy of our model we use the Mean Per Joint Position Error (MPJPE) on 3D joint coordinates, which is the most widely used metric for evaluating 3D pose errors. This metric calculates the average L2-norm across different joints between the prediction and ground truth. Since HumanML3D [14] pose representation contains 263 redundant features per body frames including joint positions, velocities and rotations we use a transformation process (described in the Appendix) to obtain the 3D joint positions in order to both calculate the MPJPE and visualize the predicted sequences.

To evaluate and compare our uncertainty indices, we use sparsification plots, a common approach for assessing how well estimated uncertainty aligns with true errors [3, 24, 28, 55]. In our implementation, we compute multiple motion sequences and rank each joint’s uncertainty. By progressively removing the joints with the highest uncertainty and summing the remaining error, we obtain the sparsification curve. The ideal reference, known as the “Oracle”, is based on ranking joints by their true errors. A well-performing and reliable uncertainty index should produce a curve that decreases monotonically and closely follows the oracle.

## 4.3. Implementation Details

Our models were trained on an *NVIDIA Titan V* GPU over 1.7 days and on *NVIDIA Tesla V100* GPU over 1.2 days with a batch size of 64. We used 8 layers of the Transformer Encoder with 4 multi-head attention for each, separated by a GeLU activation function and a dropout value of 0.1. The joint features from  $X_t$  were encoded in a latent dimension of 1024 when learning variances and 512 without learning variances. 1024 corresponds to the concatenation of the joint features of  $\hat{X}_0$  [512] and  $V_0$  [512]. To encode the text, we use a frozen CLIP-ViT-B/32 model. Each model was trained for 600K steps, after which a checkpoint was chosen that minimizes the MPJPE metric to be reported. Our generative process is conditioned by a motion input sequence of 50 frames which represents 2.5 seconds at 20FPS. We also set  $\lambda = 0.001$  to prevent  $L_{\text{VLB}}$  from overwhelming  $L_{\text{simple}}$ . We evaluate our models with guidance-scale  $\mu = 2.5$  but as discussed in the Motion & Text ablation study Section 4.4 this can be adapted for specific applications (eg. short/long-term predictions).

To evaluate the effectiveness of our multimodal fusion approach, we compare against Motion Editing baselines MotionGPT [21] and MDM [50], both of which also utilize language and motion data and are trained on Hu-

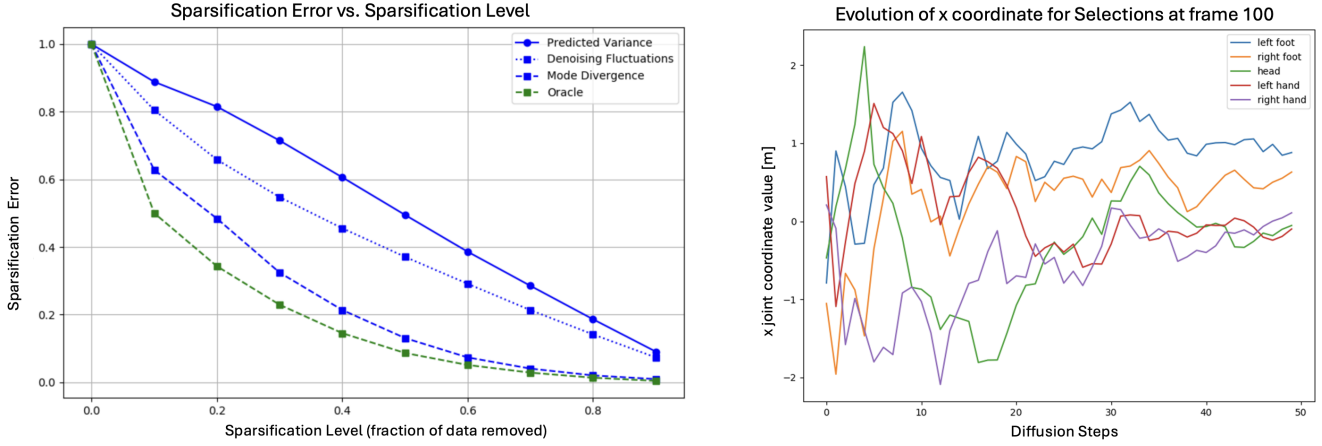


Figure 5. **(Left) Sparsification Error Plot.** Quantitative Results of the uncertainty parameters: The Mode Divergence index closely follows the Oracle curve, indicating the strongest alignment between uncertainty estimates and true errors. **(Right) Joint Position Evolution over the Denoising Process.** The position is progressively denoised until it converges to its final prediction. The fluctuations are used as a parameter for uncertainty.

manML3D [14]. We implement their pretrained versions (open-sourced) and compare on the entire test set of HumanML3D using MPJPE. To perform predictions we provide each compared model with the same motion prequel sequence (50 frames) and compare the rest of the predicted sequence to the ground truth.

#### 4.4. Quantitative & Qualitative Evaluation

**Model Accuracy Evaluation over MPJPE:** Unlike the implemented baselines MotionGPT [21] and MDM [50] that treat motion data as a masked input during sampling, our model is trained to leverage it as an additional supervision signal, which we find to lead to significantly enhances performance, especially over longer sequences. In Fig. 4 the temporal evolution chart shows that our model substantially outperforms these baselines in accuracy, with consistently lower MPJPE values over time and a more gradual increase in error compared to the sharp rise seen in MDM [50] and MotionGPT [21]. These results are also demonstrated qualitatively in the 3D plots Fig. 4 (Right) (see Appendix & Video for more examples) where our predictions align more closely with the ground truth, especially towards the end of the sequence. Indeed, both baselines' outputs fail to follow the indicated trajectory (projection of the root joint in the XZ-plane) whereas our model follows the "circle", almost aligning with the ground truth on the last frame.

**Uncertainty Parameters Evaluation:** The results of our comparison study between the different uncertainty indices are presented in Fig. 5 (Left). The Sparsification Error plot (explained in 4.2) shows that the best-performing index is the Mode Divergence, which closely follows the Oracle curve, indicating a strong alignment between uncertainty estimates and true errors. These results are also demon-

strated qualitatively in the video as well as in the Additional Experimental Results (Appendix) where we visualize the evolution of the zones of presence with varying confidence levels based on the different uncertainty indices. For clarity and visibility, we limit the uncertainty visualization to the "end-effector" joints—specifically the head, hands, and feet—since these are the most critical in human-robot collaboration, and visualizing uncertainty for all joints would create overly cluttered visuals. We calculate the mean uncertainty across the x, y, and z coordinates for each key joint, using this value as the radius of the sphere representing uncertainty around the end-effectors.

**Uncertainty Results Interpretation:** Although the Denoising Fluctuations and Predicted Variance methods show a general decline in their sparsification curves, the effect is less pronounced, suggesting these indices are less reliable for uncertainty estimation. The learned variance is supposed to generally follow the same trends as the original fixed schedule, consistently decreasing during denoising to reduce stochasticity. However, its effectiveness as an uncertainty factor is somewhat limited, as the final value, while still meaningful, becomes slightly less informative. Similarly, the instability of fluctuations diminishes their reliability. In contrast, the Mode Divergence factor consistently rises over time, aligning with the increasing error, making it the most robust and dependable indicator (see video and Appendix for visual confirmation in 3D plots).

**Ablation Study - Motion and Text Effects:** To evaluate the relevance of our multi-modal contribution, we perform an ablation study, presented in Table 1, comparing our standard approach to one where models are fed with either motion or textual inputs exclusively. Firstly, this study clearly confirms that combining both types of inputs results in sig-

Time (seconds)	0.5s	1s	1.5s	2s	2.5s	3s	3.5s	4s	4.5s	5s	5.5s
<b>Ours with motion &amp; text</b>	111.8	<b>186.7</b>	<b>267.2</b>	<b>341.8</b>	<b>408.7</b>	<b>474.8</b>	<b>540.4</b>	<b>592.5</b>	<b>629.3</b>	<b>669.8</b>	<b>705.1</b>
<b>MDM [50] with motion &amp; text</b>	192.5	337.5	479.0	604.3	716.8	820.2	906.4	976.3	1025.4	1091.9	1139.6
<b>Ours with text no motion</b>	254.8	418.6	609.5	796.8	972.2	1105.1	1253.3	1383.8	1526.1	1624.8	1679.8
<b>MDM [50] with text no motion</b>	237.9	362.6	482.9	595.5	687.8	783.2	871.6	965.3	1039.6	1085.2	1143.8
<b>Ours with motion no text</b>	<b>100.2</b>	186.9	271.9	358.9	445.7	528.6	608.7	677.6	739.1	810.8	902.0
<b>MDM [50] with motion no text</b>	406.1	614.5	852.3	1079.3	1288.6	1503.5	1684.8	1871.9	2001.6	2187.3	2332.0

Table 1. Ablation study: Motion and Text Effects

Time (seconds)	0.5s	1s	1.5s	2s	2.5s	3s	3.5s	4s	4.5s	5s	5.5s
<b>Encoder/Decoder: Linear</b>	118.6	205.5	298.8	385.5	472.0	551.3	629.7	692.0	741.0	791.9	852.1
<b>Encoder/Decoder: GCN</b>	<b>111.8</b>	<b>186.7</b>	<b>267.2</b>	<b>341.8</b>	<b>408.7</b>	<b>474.8</b>	<b>540.4</b>	<b>592.5</b>	<b>629.3</b>	<b>669.8</b>	<b>705.1</b>
<b>Learning the Variance: False</b>	<b>86.3</b>	<b>163.0</b>	<b>250.1</b>	<b>332.4</b>	409.3	485.4	560.5	622.6	676.8	729.5	775.5
<b>Learning the Variance: True</b>	111.8	186.7	267.2	341.8	<b>408.7</b>	<b>474.8</b>	<b>540.4</b>	<b>592.5</b>	<b>629.3</b>	<b>669.8</b>	<b>705.1</b>
<b>Diffusion Steps: 1000</b>	<b>104.8</b>	192.2	280.6	360.9	438.3	482.1	553.6	617.2	653.5	702.3	745.8
<b>Diffusion Steps: 50</b>	111.8	<b>186.7</b>	<b>267.2</b>	<b>341.8</b>	<b>408.7</b>	<b>474.8</b>	<b>540.4</b>	<b>592.5</b>	<b>629.3</b>	<b>669.8</b>	<b>705.1</b>

Table 2. Ablation study: Architectural Design and Parameter Choice

nificantly higher prediction accuracy. Secondly, the study indicates that our model relies more heavily on motion input sequences than textual prompts. Notably, it performs slightly better without text for very short-term predictions. This means that our model could be used in a HRC setting for continuous operation between different actions, even without specific action context. This capability is presumably not possible with Text2Motion models, which perform poorly without text, as the study shows. Finally, the study confirms that textual information is most useful for longer-term predictions where the stochasticity and variability of potential scenarios are much higher.

**Ablation Study - Architectural Design and Parameter Choice:** To assess our architectural contributions, we conduct a deeper analysis with additional ablation studies presented in Table 2. In the first study, we retrain our model with both the encoder and decoder composed of simple linear layers, as in MDM [50]. The study confirms that learnable graph connectivity improves the understanding of human joint trajectory dependencies, especially for long-term predictions. The second study evaluates our architectural design that learns the variance of the motion sample distribution. Although learning variances allow diffusion models to capture more data distribution modes with we leverage for uncertainty estimates, our study shows that it only enhance accuracy over long-term predictions. In the final study, inspired by Nichol et al. [39], we significantly reduce the number of diffusion steps from 1000 to 50 which considerably improves the computational efficiency-pivotal for real-time Human-Robot Collaboration-and resulted in improved accuracy over time.

## 5. Conclusion and Limitations

We present MDMP, a multimodal diffusion model that learns contextuality from synchronized tracked motion sequences and associated textual prompts, enabling it to predict human motion over significantly longer terms than its predecessors. Our model not only generates accurate long-term predictions but also provides uncertainty estimates, enhancing our predictions with presence zones of varying confidence levels. This uncertainty analysis was validated through a study, demonstrating the model’s capability to offer spatial awareness, which is crucial for enhancing safety in dynamic human-robot collaboration. Our method demonstrates superior results over extended durations with adapted computational time, making it well-suited for ensuring safety in Human-Robot collaborative workspaces.

A limitation of this work is the reliance on textual descriptions of actions, which can be a burden for real-time Human-Robot Collaboration, as not every action is scripted in advance. Currently, we use CLIP to embed these textual descriptions into guidance vectors for our model. An interesting future direction is to replace these descriptions with images or videos captured in real time within the robotics workspace. Since current Human Motion Forecasting methods already rely on human motion tracking data, often obtained using RGB/RGB-D cameras, the necessary material is typically already present in the workspace. Given that CLIP leverages a shared multimodal latent space between text and images, this approach could provide similar guidance while being far less restrictive, making it more practical for dynamic and unsupervised HRC environments.

## References

[1] Chaitanya Ahuja and Louis-Philippe Morency. Language2pose: Natural language grounded pose forecasting. In *International Conference on 3D Vision (3DV)*, pages 719–728. IEEE, 2019. 3

[2] Emre Aksan, Manuel Kaufmann, Peng Cao, and Otmar Hilliges. A spatio-temporal transformer for 3d human motion prediction. In *International Conference on 3D Vision (3DV)*, pages 565–574. IEEE, 2021. 3

[3] Oisin M. Aodha, Arsalan Humayun, Marc Pollefeys, and Gabriel J. Brostow. Learning a confidence measure for optical flow. *IEEE Transactions on Pattern Analysis and Machine Intelligence*, 35(5):1107–1120, May 2013. 6

[4] Yujun Cai, Lin Huang, Yiwei Wang, Tat-Jen Cham, Jianfei Cai, Junsong Yuan, Jun Liu, Xu Yang, Yiheng Zhu, Xiaohui Shen, Ding Liu, Jing Liu, and Nadia Magnenat-Thalmann. Learning progressive joint propagation for human motion prediction. In *European Conference on Computer Vision (ECCV)*, pages 226–242, 2020. 3

[5] Angelo Caregnato-Neto, Luciano Cavalcante Siebert, Arkady Zgonnikov, Marcos Ricardo Omena de Albuquerque Maximo, and Rubens Junqueira Magalhães Afonso. Armchair: integrated inverse reinforcement learning and model predictive control for human-robot collaboration, 2024. 1

[6] Xin Chen, Biao Jiang, Wen Liu, Zilong Huang, Bin Fu, Tao Chen, and Gang Yu. Executing your commands via motion diffusion in latent space. In *Proceedings of the IEEE/CVF Conference on Computer Vision and Pattern Recognition*, pages 18000–18010, 2023. 3

[7] Qiongjie Cui, Huaijiang Sun, Yue Kong, Xiaoqian Zhang, and Yanmeng Li. Efficient human motion prediction using temporal convolutional generative adversarial network. *Information Sciences*, 545:427–447, 2021. 3

[8] Qiongjie Cui, Huaijiang Sun, and Fei Yang. Learning dynamic relationships for 3d human motion prediction. In *Proceedings of the IEEE Conference on Computer Vision and Pattern Recognition (CVPR)*, pages 6519–6527, 2020. 3

[9] Prafulla Dhariwal and Alexander Nichol. Diffusion models beat gans on image synthesis. In *Advances in Neural Information Processing Systems*, volume 34, pages 8780–8794, 2021. 2

[10] Martin J. Doherty. *Theory of Mind: How Children Understand Others' Thoughts and Feelings*. Psychology Press, Hove, England, 2009. 1

[11] Katerina Fragkiadaki, Sergey Levine, Panna Felsen, and Jitendra Malik. Recurrent network models for human dynamics. In *International Conference on Computer Vision (ICCV)*, 2015. 3

[12] Liang-Yan Gui, Yu-Xiong Wang, Xiaodan Liang, and Jose M. F. Moura. Adversarial geometry-aware human motion prediction. In *Proceedings of the European Conference on Computer Vision (ECCV)*, pages 786–803, 2018. 3

[13] Chuan Guo, Yuxuan Mu, Muhammad Gohar Javed, Sen Wang, and Li Cheng. Momask: Generative masked modeling of 3d human motions. In *Proceedings of the IEEE/CVF Conference on Computer Vision and Pattern Recognition (CVPR)*, 2023. 3

[14] Chuan Guo, Shihao Zou, Xinxin Zuo, Sen Wang, Wei Ji, Xingyu Li, and Li Cheng. Generating diverse and natural 3d human motions from text. In *IEEE/CVF Conference on Computer Vision and Pattern Recognition (CVPR)*, pages 5152–5161, 2022. 3, 5, 6, 7, 12

[15] Chuan Guo, Xinxin Zuo, Sen Wang, Shihao Zou, Qingyao Sun, Annan Deng, Minglun Gong, and Li Cheng. Action2motion: Conditioned generation of 3d human motions. In *Proceedings of the 28th ACM International Conference on Multimedia* 2021–2029, 2020. 5

[16] Alejandro Hernandez, Jurgen Gall, and Francesc Moreno-Noguer. Human motion prediction via spatio-temporal inpainting. In *Proceedings of the IEEE International Conference on Computer Vision (ICCV)*, pages 7134–7143, 2019. 3

[17] Jonathan Ho, Ajay Jain, and Pieter Abbeel. Denoising diffusion probabilistic models. In *Advances in Neural Information Processing Systems*, volume 33, pages 6840–6851, 2020. 2, 4

[18] Jonathan Ho and Tim Salimans. Classifier-free diffusion guidance. *arXiv preprint arXiv:2207.12598*, 2022. 2

[19] Jonathan Ho, Tim Salimans, Alexey Gritsenko, William Chan, Mohammad Norouzi, and David J Fleet. Video diffusion models. *arXiv:2204.03458*, 2022. 2

[20] Ashesh Jain, Amir R. Zamir, Silvio Savarese, and Ashutosh Saxena. Structural-rnn: Deep learning on spatio-temporal graphs. In *Conference on Computer Vision and Pattern Recognition (CVPR)*, 2016. 3

[21] Biao Jiang, Xin Chen, Wen Liu, Jingyi Yu, Gang Yu, and Tao Chen. Motiongpt: Human motion as a foreign language. *Advances in Neural Information Processing Systems*, 36, 2024. 3, 6, 7, 13

[22] QiuHong Ke, Mohammed Bennamoun, Hossein Rahmani, Senjian An, Ferdous Sohel, and Farid Boussaid. Learning latent global network for skeleton-based action prediction. *IEEE Transactions on Image Processing*, 29:959–970, 2019. 3

[23] Diederik P Kingma and Max Welling. Auto-encoding variational bayes. *arXiv preprint arXiv:1312.6114*, 2013. 4

[24] Christian Konermann, Rudolf Mester, and Christoph Garbe. A statistical confidence measure for optical flows. In *Pattern Recognition*, pages 290–301. Springer Berlin Heidelberg, Berlin, Heidelberg, 2008. 6

[25] Aadi Kothari, Tony Tohme, Xiaotong Zhang, and Kamal Youcef-Toumi. Enhanced human-robot collaboration using constrained probabilistic human-motion prediction, 2023. 1

[26] Hsu kuang Chiu, Ehsan Adeli, Borui Wang, De-An Huang, and Juan Carlos Niebles. Action-agnostic human pose forecasting. In *IEEE Winter Conference on Applications of Computer Vision (WACV)*, 2019. 3

[27] Jogendra Nath Kundu, Maharsi Gor, and R. Venkatesh Babu. Bihmp-gan: Bidirectional 3d human motion prediction gan. In *Proceedings of the AAAI Conference on Artificial Intelligence*, volume 33, pages 8553–8560, 2019. 3

[28] Jan Kybic and Clemens Nieuwenhuis. Bootstrap optical flow confidence and uncertainty measure. *Computer Vision and Image Understanding*, 115(10):1449–1462, 2011. 6

[29] Fanjia Li, Aichun Zhu, Yonggang Xu, Ran Cui, and Gang Hua. Multi-stream and enhanced spatial-temporal graph convolution network for skeleton-based action recognition. *IEEE Access*, 8:97757–97770, 2020. 3

[30] Maosen Li, Siheng Chen, Yangheng Zhao, Ya Zhang, Yanfeng Wang, and Qi Tian. Dynamic multiscale graph neural networks for 3d skeleton based human motion prediction. In *Proceedings of the IEEE Conference on Computer Vision and Pattern Recognition (CVPR)*, pages 214–223, 2020. 3

[31] Xiaoli Liu, Jianqin Yin, Jin Liu, Pengxiang Ding, Jun Liu, and Huaping Liub. Trajectorycnn: A new spatio-temporal feature learning network for human motion prediction. *IEEE Transactions on Circuits and Systems for Video Technology*, 2020. 3

[32] Zhenguang Liu, Shuang Wu, Shuyuan Jin, Qi Liu, Shijian Lu, Roger Zimmermann, and Li Cheng. Towards natural and accurate future motion prediction of humans and animals. In *Conference on Computer Vision and Pattern Recognition (CVPR)*, 2019. 3

[33] Ziyu Liu, Hongwen Zhang, Zhenghao Chen, Zhiyong Wang, and Wanli Ouyang. Disentangling and unifying graph convolutions for skeleton-based action recognition. In *Proceedings of the IEEE/CVF Conference on Computer Vision and Pattern Recognition*, pages 143–152, 2020. 3

[34] Calvin Luo. Understanding diffusion models: A unified perspective. *arXiv preprint arXiv:2208.11970*, 2022. 3

[35] Naureen Mahmood, Nima Ghorbani, Nikolaus F. Troje, Gerard Pons-Moll, and Michael J. Black. Amass: Archive of motion capture as surface shapes. In *International Conference on Computer Vision*, pages 5442–5451, October 2019. 5

[36] Wei Mao, Miaomiao Liu, Mathieu Salzmann, and Hongdong Li. Learning trajectory dependencies for human motion prediction. In *International Conference on Computer Vision (ICCV)*, pages 9488–9496, 2019. 2, 3, 5

[37] Julieta Martinez, Michael J. Black, and Javier Romero. On human motion prediction using recurrent neural networks, 2017. 3

[38] Angel Martinez-Gonzalez, Michael Villamizar, and Jean-Marc Odobez. Pose transformers (potr): Human motion prediction with non-autoregressive transformers. In *International Conference on Computer Vision Workshops (ICCVW)*, pages 2276–2284, 2021. 3

[39] Alex Nichol and Prafulla Dhariwal. Improved denoising diffusion probabilistic models. In *International Conference on Machine Learning*, 2021. 2, 4, 5, 8

[40] Alex Nichol, Prafulla Dhariwal, Aditya Ramesh, Pranav Shyam, Pamela Mishkin, Bob McGrew, Ilya Sutskever, and Mark Chen. Glide: Towards photorealistic image generation and editing with text-guided diffusion models. *arXiv preprint arXiv:2112.10741*, 2021. 2

[41] Mathis Petrovich, Michael J. Black, and Gul Varol. Temos: Generating diverse human motions from textual descriptions. In *European Conference on Computer Vision (ECCV)*, 2022. 3

[42] Ekkasit Pinyoanuntapong, Pu Wang, Minwoo Lee, and Chen Chen. Mmm: Generative masked motion model. In *Proceedings of the IEEE/CVF Conference on Computer Vision and Pattern Recognition (CVPR)*, 2024. 3

[43] V. Popov, I. Vovk, V. Gogoryan, T. Sadekova, and M. Kudinov. Grad-tts: A diffusion probabilistic model for text-to-speech. In *International Conference on Machine Learning*, pages 8599–8608. PMLR, 2021. 2

[44] Alec Radford, Jong Wook Kim, Chris Hallacy, Aditya Ramesh, Gabriel Goh, Sandhini Agarwal, Girish Sastry, Amanda Askell, Pamela Mishkin, Jack Clark, et al. Learning transferable visual models from natural language supervision. In *International Conference on Machine Learning*, pages 8748–8763. PMLR, 2021. 2, 3, 4

[45] Aditya Ramesh, Prafulla Dhariwal, Alex Nichol, Casey Chu, and Mark Chen. Hierarchical text conditional image generation with clip latents. *arXiv preprint arXiv:2204.06125*, 2022. 4

[46] Jascha Sohl-Dickstein, Eric Weiss, Niru Maheswaranathan, and Surya Ganguli. Deep unsupervised learning using nonequilibrium thermodynamics. In *International Conference on Machine Learning*, pages 2256–2265. PMLR, 2015. 2

[47] Jiaming Song, Chenlin Meng, and Stefano Ermon. Denoising diffusion implicit models. *arXiv preprint arXiv:2010.02502*, 2020. 2

[48] Jiaming Song, Chenlin Meng, and Stefano Ermon. Denoising diffusion implicit models. *arXiv:2010.02502*, October 2020. 2

[49] Yang Song, Prafulla Dhariwal, Mark Chen, and Ilya Sutskever. Consistency models. In *Proceedings of the 40th International Conference on Machine Learning, ICML’23*. JMLR.org, 2023. 2

[50] Guy Tevet, Sigal Raab, Brian Gordon, Yoni Shafir, Daniel Cohen-or, and Amit Haim Bermano. Human motion diffusion model. In *The Eleventh International Conference on Learning Representations*, 2023. 2, 3, 4, 6, 7, 8, 13

[51] Ashish Vaswani, Noam Shazeer, Niki Parmar, Jakob Uszkoreit, Llion Jones, Aidan N Gomez, Łukasz Kaiser, and Illia Polosukhin. Attention is all you need. In *Advances in Neural Information Processing Systems*, volume 30, 2017. 3, 5

[52] Petar Veličković, Guillem Cucurull, Arantxa Casanova, Adriana Romero, Pietro Lio, and Yoshua Bengio. Graph attention networks. In *International Conference on Learning Representations (ICLR)*, 2018. 5

[53] Dong Wang, Yuan Yuan, and Qi Wang. Early action prediction with generative adversarial networks. *IEEE Access*, 7:35795–35804, 2019. 3

[54] Jiashun Wang, Huazhe Xu, Medhini Narasimhan, and Xiaolong Wang. Multi-person 3d motion prediction with multi-range transformers. In *Advances in Neural Information Processing Systems (NeurIPS)*, pages 6036–6049, 2021. 3

[55] Alexander S. Wannenwetsch, Margret Keuper, and Stefan Roth. Probflow: Joint optical flow and uncertainty estimation. In *IEEE International Conference on Computer Vision (ICCV)*, Oct 2017. 6

[56] Dongchao Yang, Jianwei Yu, Helin Wang, Wen Wang, Chao Weng, Yuexian Zou, and Dong Yu. Diffsound: Discrete

diffusion model for text-to-sound generation. *IEEE/ACM Transactions on Audio, Speech, and Language Processing*, 31:1720–1733, 2023. 2

[57] Hao Yang, Chunfeng Yuan, Li Zhang, Yunda Sun, Weiming Hu, and Stephen J. Maybank. Sta-cnn: Convolutional spatial-temporal attention learning for action recognition. *IEEE Transactions on Image Processing*, 29:5783–5793, 2020. 3

[58] Dianhao Zhang, Mien Van, Pantelis Sopasakis, and Seán McLoone. An nmpc-ecbf framework for dynamic motion planning and execution in vision-based human-robot collaboration, 2023. 1

[59] Xikun Zhang, Chang Xu, and Dacheng Tao. Context aware graph convolution for skeleton-based action recognition. In *2020 IEEE/CVF Conference on Computer Vision and Pattern Recognition (CVPR)*, pages 14321–14330, 2020. 3

[60] Tianhang Zheng, Sheng Liu, Changyou Chen, Junsong Yuan, Baochun Li, and Kui Ren. Towards understanding the adversarial vulnerability of skeleton-based action recognition. *arXiv preprint arXiv:2005.07151*, 2020. 3

## Supplementary Material

### A. Experiment Setup

We provide details about our experimental setup used in our lab to predict the future motions of a human worker in a Human-Robot Collaborative (HRC) Workspace.

**Physical Setup:** Our collaborative workspace, as shown in Fig. 1, consists of a duAro1 Kawasaki robot and multiple desks where both the human and the robot can place and pass objects. The workspace is monitored by multiple Azure Kinect RGB-D cameras. All sensor data, along with the command signals for controlling the robot, are centralized in a ROS (Robot Operating System) setup. April Tags are used for calibration to ensure all spatial data (including the real-time position of the robot and data from the sensors) is aligned within the same reference frame.

**Motion Tracking:** Human Pose Estimation is performed in real-time to gather skeleton data and track the human worker within the HRC workspace using the Azure Kinect Body Tracking SDK. The skeleton data is transmitted to the ROS system via the Azure Kinect ROS driver, transformed into the robot’s base frame, and then recorded in MarkerArray topics. These motion sequences are subsequently fed into our trained model.

**Textual Actions:** To leverage the benefits of our multi-modal approach, a set of predefined Human-Robot collaborative actions is mapped to specific keys on a keyboard. This keyboard can be operated by either the human worker or an external observer who can also provide detailed textual descriptions of the actions being performed. If the model is not given textual information between actions, it relies solely on motion sequence data. As demonstrated in our Motion & Text ablation study in section C, our model can perform short-term predictions without contextual information.

This setup allows us to accurately capture and predict the future motions of human workers, enhancing the efficiency and safety of the HRC workspace.

### B. Data Processing for Visualization, Evaluation, and Training

This paragraph provides detailed information on the data processing steps used in our study. Specifically, it covers the feature transformation process necessary to handle the pose representation in the HumanML3D [14] dataset and the adaptation of our model to work with 3D joint position data captured in real-time.

#### B.1. Feature Transform

In our work, feature transform is a crucial step to obtain the 3D joint positions from the pose representation provided by the HumanML3D [14] dataset. This transforma-

tion is necessary because the dataset’s pose representation includes a variety of redundant features that must be processed to isolate the 3D joint coordinates required for quantitative evaluation of the model using the Mean Per Joint Position Error (MPJPE) and for qualitative evaluation through visualization of the predicted sequences (see section C and video presentation).

The pose representation in HumanML3D [14] (described in the paper) consists of a tuple of features including root angular velocity, root linear velocities, root height, local joints positions, velocities, rotations, and binary foot contact features. Specifically, it provides 263 features per body frame. These features include information such as joint positions, velocities, and rotations in root space, which need to be transformed to extract the 3D joint positions.

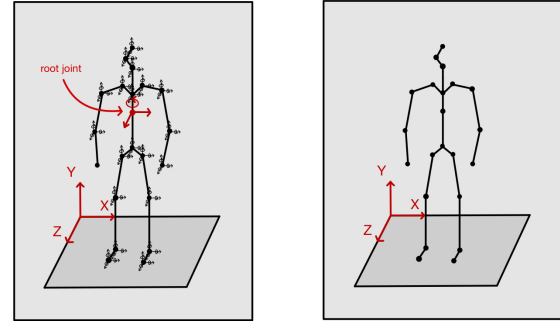


Figure 6. **Human Pose Representation.** (Left) HumanML3D features. (Right) 3D joint positions.

The transformation process involves the following steps:

1. **Recover Root Rotation and Position:** First, the root rotation velocities are extracted and integrated over time to get the root rotation angles. These angles are then converted into quaternions. Simultaneously, the root positions are recovered by integrating the root linear velocities.

2. **Concatenate Rotations and Positions:** The local joint rotations and positions, provided in the dataset, are combined with the root rotations. The combined rotations are converted from quaternion representation to a continuous 6D rotation format.

3. **Forward Kinematics:** Using forward kinematics, the combined rotations and positions are processed to obtain the global 3D joint positions. This involves computing the global position of each joint based on its local rotation and position relative to the root and applying the root’s global transformation.

## B.2. Adaptation to 3D Joint Position Data

Due to the nature of our recorded motion capture data using real-time pose estimation, the pose data we have access to consists only of 3D joint positions. This results in a simplified feature representation of 96 features per skeleton (32 joints  $\times$  3 coordinates) instead of the 263 features per body frame provided by the HumanML3D dataset. To address this discrepancy, we considered two potential solutions:

1. **Transformation to Original Feature Space:** One approach was to transform the 3D joint positions back to the original feature space of 263 features per skeleton. However, this transformation involves estimating several parameters that are not directly observable from the joint positions alone which will likely introduce inaccuracies into the data, that could negatively impact the model’s performance. For instance, approximating the root angular velocity can be complex and computing local rotations typically requires sophisticated methods like inverse kinematics (IK).

2. **Retraining the Model:** Instead of transforming the data, we opted to retrain the model using the simplified feature representation of 3D joint positions. The only modifications involved are the dimensions of the Encoder and Decoder. By training directly on the motion sequences represented as 3D joint positions, we avoid the inaccuracies associated with the transformation process and ensure that the model is trained on the most accurate representation of our data. However, the redundant pose representation can be useful to learn spatio-temporal motion patterns, and this lower-dimensional pose representation might result in a slight loss of information that could potentially decrease the model’s performance. Another consideration is that the pose estimation data we access through pose estimation includes 32 joints, whereas the HumanML3D dataset uses only 22 joints to represent the human body. Therefore, we need to filter out the 10 additional joints and predict motion sequences using only the 22 joints per frame.

We chose the second approach and retrained our model on the 3D joint position feature space. This retrained model was then used for the experiments in our lab, allowing us to work directly with the data collected through our real-time pose estimation system.

## C. Additional Experimental Results

We present qualitative results by comparing our model to state-of-the-art Text2Motion methods such as MotionGPT [21] and MDM [50]. The comparisons are showcased in the video appendix, where our model’s predictions are visualized against ground truth motion sequences. In every sequence, our model outperforms both MDM and MotionGPT in terms of proximity to the ground truth and adherence to the semantic content of the textual action prompts. Even when our predicted sequences differ from

the ground truth, the actions correspond accurately to the textual descriptions, whereas both baselines quickly diverge from the ground truth.

Additionally, we visualize our predictions using meshes created with SMPL and rendered in Blender. These visualizations transform the skeleton motions into human-like meshes performing the same actions, providing a clearer and more intuitive understanding of the predicted motions.

## C.1. Video Representation

In the video appendix, we compare our model’s predictions to those of MDM and MotionGPT on certain specific actions. The videos allow for a visual assessment of the proximity of the predicted sequences to the ground truth motion. Our model shows better performance in maintaining proximity to the ground truth and in following the semantics of the textual action prompts. Even when the predictions differ from the ground truth, our model’s predicted actions align with the intended textual actions, while the baseline models tend to diverge.

## C.2. Path Trajectory Following

In Fig. 7, we also evaluate the trajectory following capability of our model through stop-motion images. These images track the motion sequences with faded colors for early frames and progressively darker colors for later frames. Additionally, a trajectory path projecting the root joint position on the XZ-plane is included to precisely follow the predicted trajectory. This study further confirms our model’s ability to accurately predict motion sequences that follow precise trajectories over long-term durations.

## C.3. Additional Uncertainty Qualitative Comparison

In Figs. 8, 9, 10, and 11, we present additional results of our Uncertainty Parameters for visual comparison and evaluation. As shown in these figures, the “Mode Divergence” index is the only one that exhibits a notable increase over time, correlating closely with the error, particularly when the divergence between the prediction and ground truth becomes pronounced (see Figs. 8 and 11). In contrast, the “Predicted Variance” shows less temporal variation, while the “Mean Fluctuations” appear somewhat more unstable. These findings align with our previous analysis using the Sparsification Plot in Fig. 5.

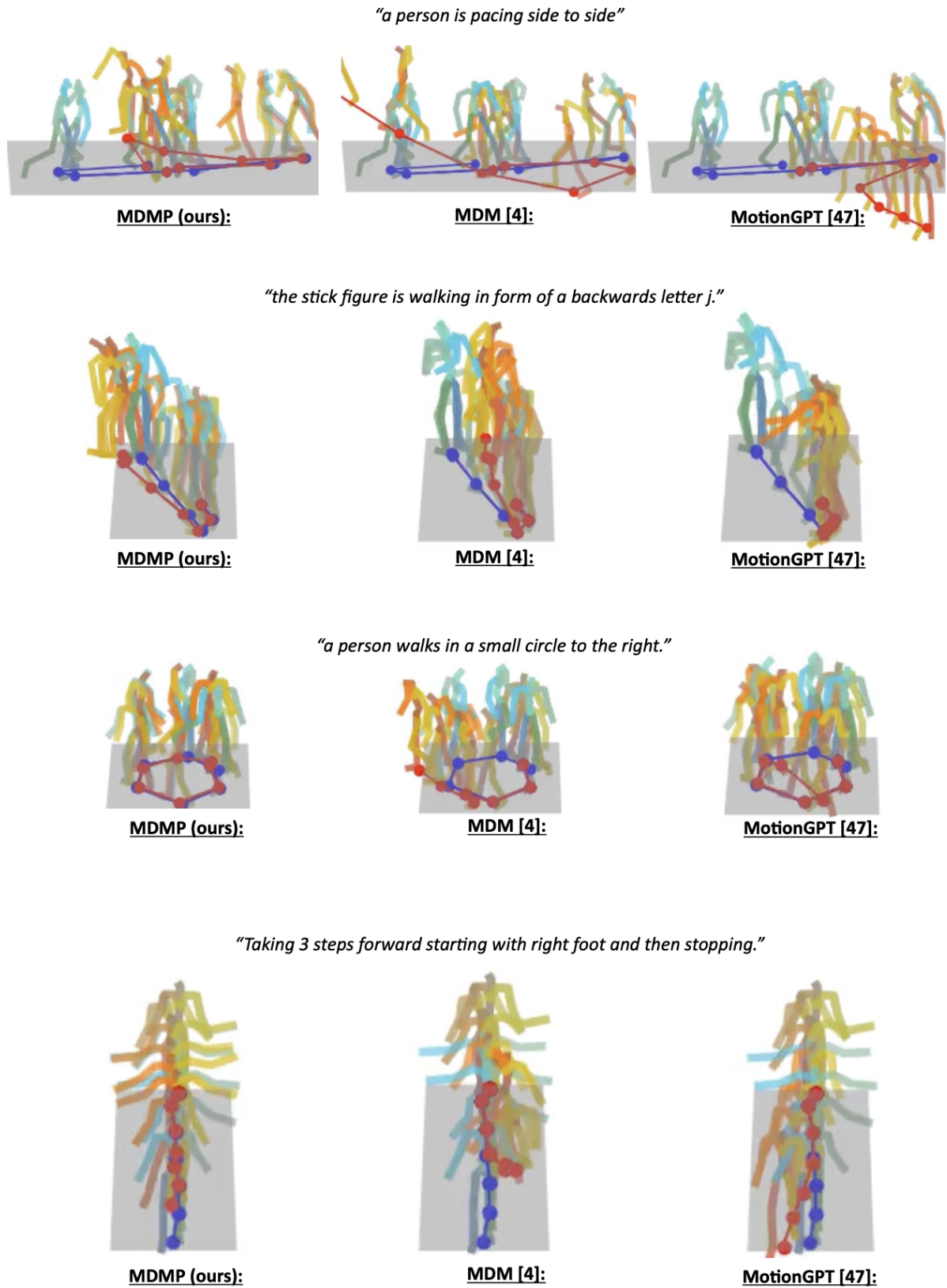


Figure 7. **Qualitative Comparisons on Path Following.** Ground-truth in **red**; Predictions in **blue**

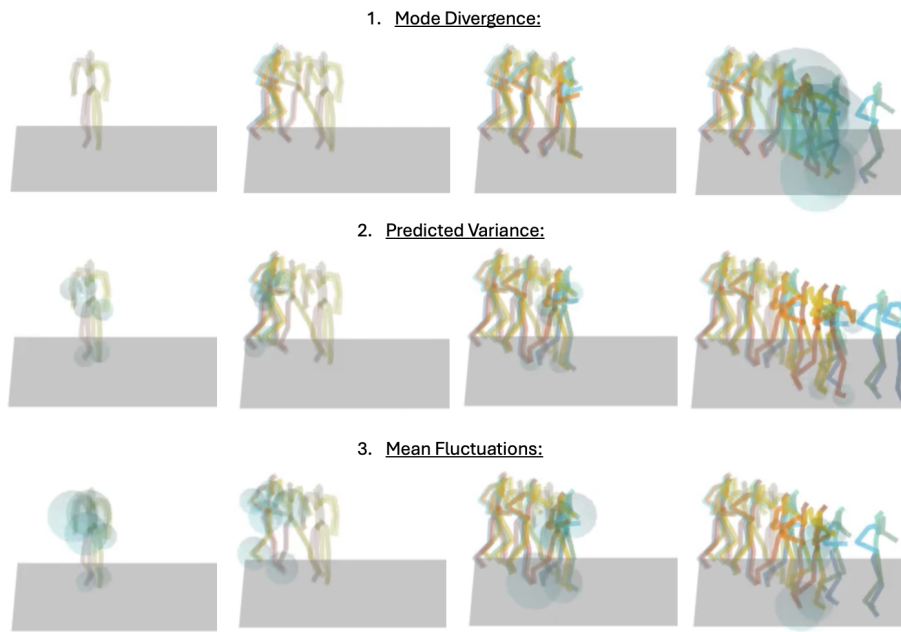


Figure 8. **Qualitative Comparisons on Uncertainty Parameters.** Textual Prompt: "a person is jogging back and forth from where he has standing"; Ground-truth in **red**; Predictions in **blue**

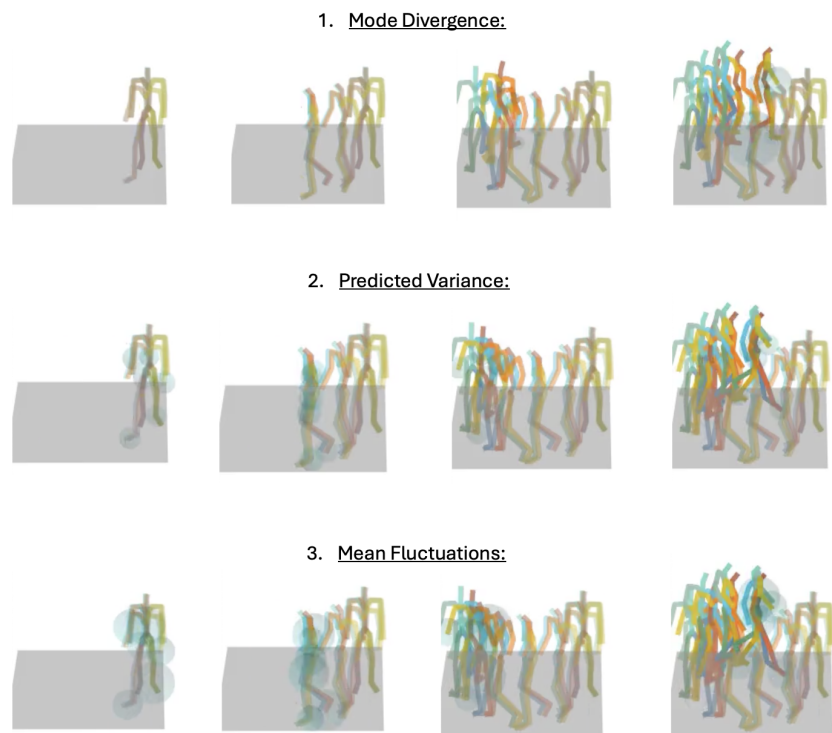


Figure 9. **Qualitative Comparisons on Uncertainty Parameters.** Textual Prompt: "a person walks in a circle, clockwise."; Ground-truth in **red**; Predictions in **blue**

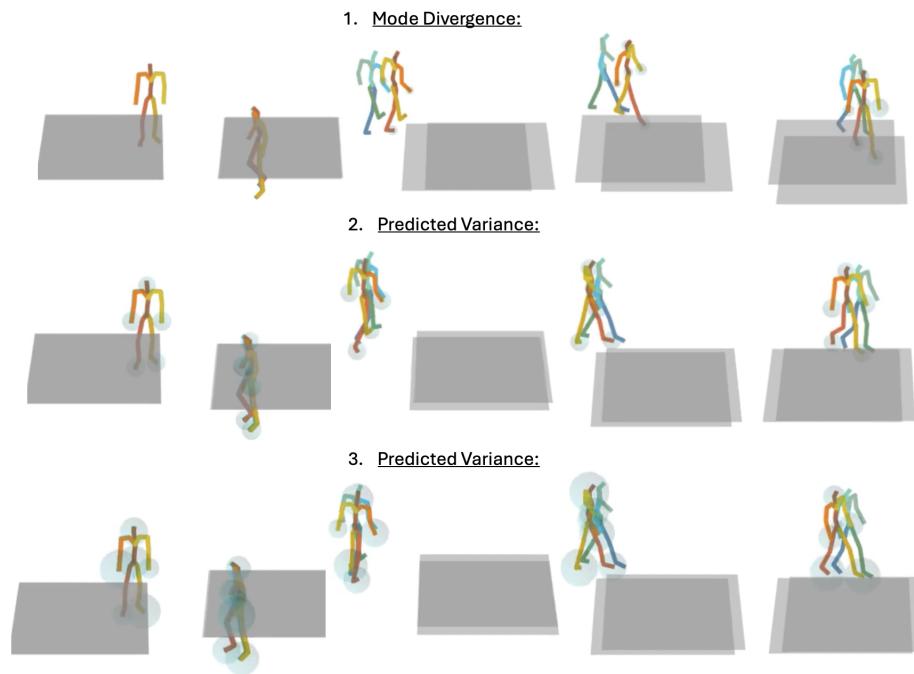


Figure 10. **Qualitative Comparisons on Uncertainty Parameters.** Textual Prompt: "a person walks around in a circle."; Ground-truth in **red**; Predictions in **blue**

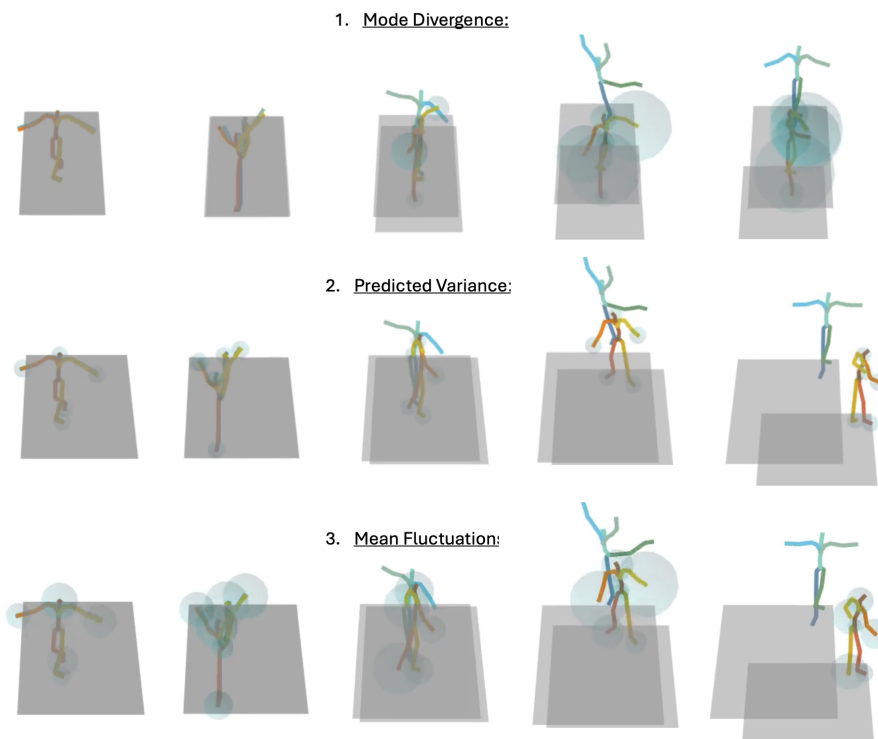


Figure 11. **Qualitative Comparisons on Uncertainty Parameters.** Textual Prompt: "a person is doing a acrobatic dance."; Ground-truth in **red**; Predictions in **blue**